Photoinduced Energy- and Electron- Transfer Between a Photoactive Cage Based on a Thermally Activate Delayed Fluorescence Ligand and Encapsulated Fluorescent Dyes

Diego Rota Martir,[a] Antonella Pizzolante,[a] Daniel Escudero,[b] Denis Jacquemin,[b] Stuart L. Warriner,[c] and Eli Zysman-Colman[a]**

[a] Organic Semiconductor Centre, EaStCHEM School of Chemistry, University of St Andrews, St Andrews, Fife, UK, KY16 9ST, Fax: +44-1334 463808; Tel: +44-1334 463826; E-mail: eli.zysman-colman@st-andrews.ac.uk;
[b] CEISAM UMR CNRS 6230, Université de Nantes, 2 rue de la Houssinière, BP 92208, 44322 Nantes Cedex 3, France; E-mail: Denis.Jacquemin@univ-nantes.fr;
[c] School of Chemistry, University of Leeds, Woodhouse Lane, Leeds, LS2 9JT, UK.

Keywords: photoactive cage, TADF ligand, encapsulation of dyes, energy and electron transfer, white-emitting assembly.

Abstract. The vast majority of polyhedral assemblies prepared by combining organic bent ligands and "photophysically innocent" palladium(II) metal ions are non-emissive. Here we report a simple strategy to switch on the luminescence properties of a polyhedral assembly by combining a Thermally Activated Delayed Fluorescence (TADF) organic emitter based on a dipyridylcarbazole ligand scaffold with Pd^{2+} ions, giving rise to a luminescent Pd_6L_{12} molecular cube. The assembly is capable of encapsulating within its cavity up to three molecules per cage of Fluorescein, in its neutral lactone form, and up to two molecules of Rose Bengal in its dianionic quinoidal form. Photoinduced electron Transfer (PeT) between the photoactive cage and the encapsulated Fluorescein and Photoinduced Energy Transfer (PET) from the cage to encapsulated Rose Bengal have been observed by steady-state and time-resolved emission spectroscopy.

Introduction.

Coordination cages, formed through the self-assembly of arrays of metal ions and bridging ligands, have been one of the main areas of interest in supramolecular chemistry during the last two decades.[1-4] More recently, the focus has turned towards the functional properties of such cages.[5-8] Small guest molecules have been shown to be sequestered inside the cavities of these cages and their host-guest interactions have been exploited in diverse applications such as in sensing,[9] for gas storage and purification,[10] and for catalysis.[11-12]

In recent years, there has been an increasing exploration of the properties of photoactive supramolecular cages in which at least one component, either the metal ion[13-15] or the bridging ligand,[16-18] is luminescent. Such cages provide both a high concentration of luminophoric units in known relative orientations and dispositions, and restricted shape and size to govern the host-guest interactions. There are only a few examples of photoactive cages based on palladium(II) metal ions.[19-21] More generally, incorporation of fluorescent emitters such as porphyrins,[22] BODIPYs,[23] and π-conjugated organic compounds,[16-17] or phosphorescent complexes such as iridium(III),[24-26]ruthenium(II),[27-29]and platinum(II)[30-31] metal complexes either into the ligand backbone or as coordinating vertices of the cage have all been previously explored. The luminescent properties of these assemblies have been primarily exploited for small molecules sensing,[23,32-33] biological imaging,[34] and photoresponsive guest uptake/release.[35-36] However, the vast majority of cage structures composed of organic bridging ligands coordinated to $Pd^{(II)}$ or $Pt^{(II)}$ are non-emissive. For instance, the self-assembly of 3,6-bis(pyridin-4-ylethynyl)-carbazole ligand, L, with Pd^{2+} ions gave rise to non-emissive cages of compositions $[Pd_2L_4]^{4+}$ and $[Pd_4L_8]^{8+}$.[37]

Depending on the nature of the emission, luminescence emanating from a single species can be broadly classified into three main categories: fluorescence, phosphorescence and thermally activated delayed fluorescence (TADF). Among these three mechanisms, purely organic TADF compounds have recently attracted attention as sustainable, inexpensive, and

efficient emitters in Organic Light-Emitting Devices (OLEDs).[38-40]In the OLED, similar to phosphorescent organometallic emitters, TADF compounds can harvest both singlet and triplet excitons for light emission via a thermal upconversion of the triplet excitons to singlet excitons mediated by a reverse intersystem crossing (RISC). TADF relies on a small (< 0.2 eV) singlet-triplet energy gap, ΔE_{ST}, defined as the difference in energy between the lowest energy triplet state (T_1) and the lowest energy singlet state (S_1). These emitters are generally based on donor-acceptor structures in which the donor moieties are in a highly twisted conformation relative to the acceptors plane, resulting in reduced exchange integral between the HOMO and LUMO and therefore small ΔE_{ST}.[41-42]

Herein we report the first example of self-assembly involving an organic TADF ligand, **4PyCzBP**, with Pd^{2+} ions, which gives rise to a luminescent cage of composition [(**4PyCzBP**)$_{12}$Pd$_6$](BF$_4$)$_{12}$, **4PyCzBP-Pd** (Figure **1**). **4PyCzBP** itself is based on a 3,6-di(pyridin-4-yl)-*9H*-carbazole donor moiety and ligand scaffold functionalised with benzophenone as the acceptor unit. The photoactive cage **4PyCzBP-Pd** is capable of encapsulating two common xanthene-based dyes, Fluorescein, in its neutral lactone form, and Rose Bengal, in its dianionic quinoidal form. Photoinduced electron Transfer (PeT) between the photoactive cage and the encapsulated Fluorescein, and Photoinduced Energy Transfer (PET) from the cage to the encapsulated Rose Bengal have been observed by steady-state and time-resolved emission spectroscopy.

Results and discussion.

We recently reported the syntheses and the photophysical properties of **4PyCzBP** and **3PyCzBP** (4-(3,6-di(pyridin-3,4-yl)-9*H*-carbazol-9-yl)phenyl)(phenyl)methanone), the former of which was used to make two component supramolecular gels.[43] The TADF nature of

4PyCzBP and **3PyCzBP** was confirmed through a combination of steady-state and time-resolved emission spectroscopy measurements.[43-44]

When **4PyCzBP** and $[Pd(NCMe)_4](BF_4)_2$ were heated in a 2:1 ratio in DMSO-d_6 at 85ºC for 12 h the proton resonances associated with **4PyCzBP** broadened and shifted downfield (Figure **1a**). The broad ^{1}H NMR signals are indicative of the formation of a large structure, the motion of which being very slow on the NMR time scale (Figure **1b**). Evidence for the formation of a single species was confirmed by ^{1}H DOSY NMR spectroscopy where the diffusion coefficient, D, in DMSO-d_6 was found to be 9.1×10^{-11} m^2/s. The magnitude of D correlates to the presence of a larger structure than the **4PyCzBP** ligand, which shows a diffusion coefficient of 1.7×10^{-10} m^2/s (Figure **1c**).

The calculated hydrodynamic radius (r_s) of the cage is 12.1 Å (Table **S1**). The compositions of the assembly **4PyCzBP-Pd** has been unequivocally established to be $[(\mathbf{4PyCzBP})_{12}Pd_6](BF_4)_{12}$ by HR-ESI-MS spectrometry, showing isotopically resolved peaks for $[(\mathbf{4PyCzBP\text{-}Pd})\text{-}(BF_4)_n]^{n+}$ (n = 5 - 8) (Figures **2** and **S5**–**S8**). The angle between the two 4-pyridyl coordinating motifs in **4PyCzBP** is 93.5°, which is ideal for the formation of a Pd_6L_{12} cage (Figure **S2**). Indeed, Fujita *et al*. previously reported that the formation of Pd_6L_{12} assemblies is only possible when the pyridine-based ligands have angles of approximately 90°.[45-46]Under similar reaction conditions, the self-assembly of **3PyCzBP** with $[Pd(NCMe)_4](BF_4)_2$ produced multiple products including the assembly of composition $[(\mathbf{3PyCzBP})_4Pd_2](BF_4)_4$, which was detected by ESI-HR-MS spectrometry (Figures **S9**-**S12**).

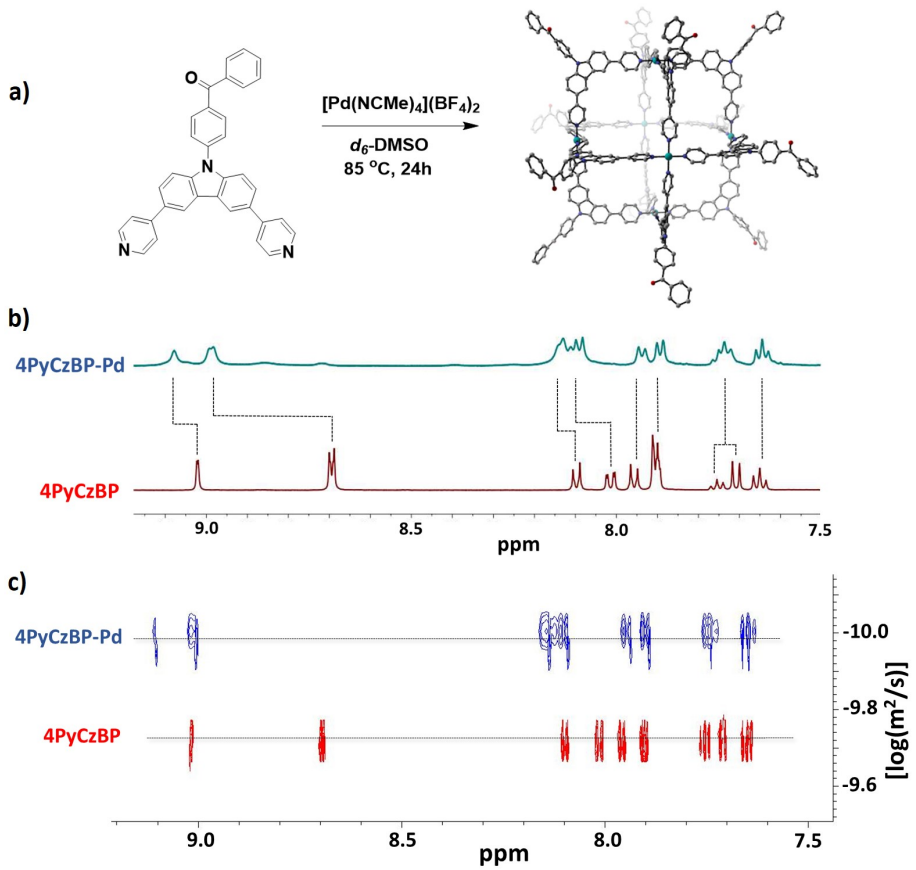

Figure **1. a)** Self-assembly between **4PyCzBP**, and Pd^{2+} ions yielding cage **4pyCzBP-Pd**. The geometries of **4pyCzBP-Pd** has been determined in *vacuo* with DFT. **b)** ^{1}H NMR of **4PyCzBP**, in red and **4PyCzBP-Pd**, in blue. **c)** ^{1}H DOSY NMR of **4PyCzBP**, in red and **4PyCzBP-Pd**, in blue. The NMR spectra were collected in DMSO-d_6 at 298 K.

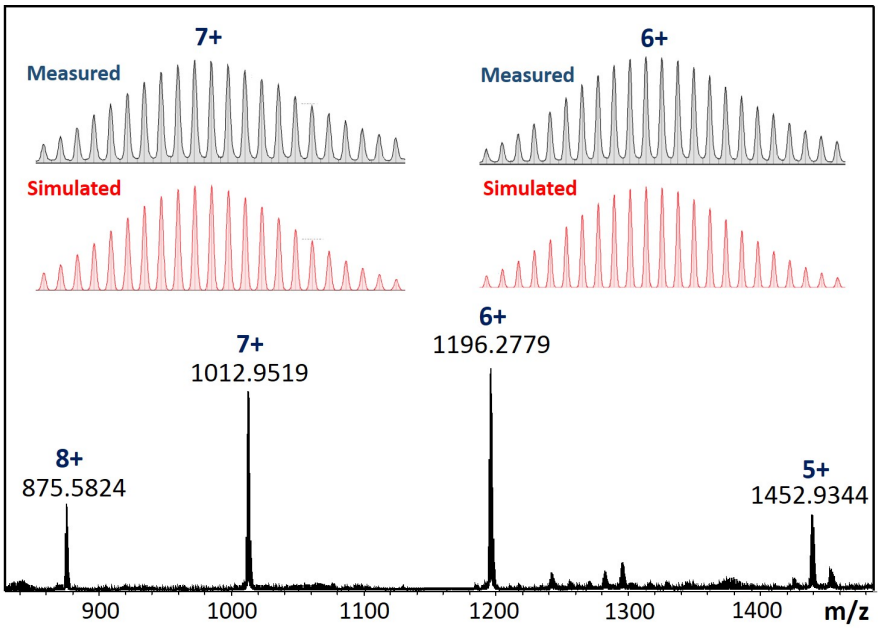

Figure **2**. ESI-MS spectra of a DMSO solution containing cage **4PyCzBP-Pd**. Inserts show the measured (in blue) and simulated (in red) isotope patterns for the 7+ (left) and 6+ (right) charge states. Additional data is given in the supporting information.

The structures of **4PyCzBP-Pd** was modelled at the B3LYP-D3^{BJ}/6-31G(d)/LanL2DZ level of theory (Figure **1a**). The computed structure of Pd_6L_{12} cube places the six Pd ions at the center of each face of the cube in a structure close to D_2 point group. Similar cubic assemblies of compositions M_6L_{12} and $M_{12}L_{12}$ have been previously reported.[45,47-49] The dimension of the optimized structure of **4PyCzBP-Pd** is *ca*. 4 x 4 x 4 nm, corresponding to a volume of *ca*. 6400 Å^3. The diameter of **4PyCzBP-Pd**, based on the Pd···Pd distance, is *ca*. 21.6 Å, whereas its diameter around the macrocyclic core across long axes of the structure is 47.8 Å (Figure **S2**). The dimensions of **4PyCzBP-Pd** are comparable to those of the Pd_6L_{12} nanocube of Fujita *et al*.,[45] and of the $Cu_{12}L_{12}$ truncated octahedron of Yaghi *et al*.,[47] which showed, respectively, diameters of 26.0 Å and 27.0 Å. The nanostructure of the cage was probed by Transmission Electron Microscopy (TEM) measurements upon deposition of a 1 x 10^{-6} M DCM solution of **4PyCzBP-Pd** onto carbon-coated copper grids (Figure **3**). The size of the nanostructures range between 4.5 – 5.0 nm and matches with the diameter of 4.78 nm obtained for the calculated structure (Figure **S2**).

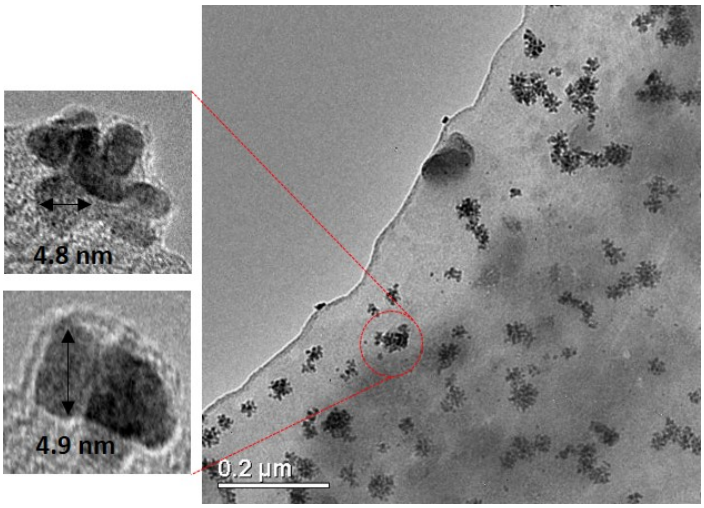

Figure **3**. TEM images of the nanostructures of **4PyCzBP-Pd**.

The emission profile of **4PyCzBP-Pd** in DCM (Figure **4a**) is broader and red-shifted at 555 nm with a lower photoluminescence quantum yield, Φ_{PL}, of 4% compared to that of **4PyCzBP** (λ_{max} = 477 nm, Φ_{PL} = 52%).[43]Similarly, the emission of **4PyCzBP-Pd** in PMMA-doped film is red-shifted at 553 nm with a Φ_{PL} of 5% compared to the emission observed for **4PyCzBP** (λ_{max} = 447 nm, Φ_{PL} = 21%). The emission decay profile of **4PyCzBP** and **4PyCzBP-Pd** collected in DCM solution and as PMMA-doped films at 298 K are illustrated in Figure **4b**. As previously reported, the transient PL decay in DCM of **4PyCzBP** is triexponential showing a short prompt fluorescence, τ_p, of 15.1 ns and a longer two-component delayed fluorescence, τ_d, of 0.69 μs and 9.80 μs. Similarly, in the PMMA doped film **4PyCzBP** exhibits a τ_p of 33.5 ns and τ_d of 0.61 μs and 6.32 μs. The cage **4PyCzBP-Pd** does not exhibit a delayed fluorescence either in DCM solution or as a PMMA-doped film. **4PyCzBP-Pd** exhibits a bi-exponential fluorescence decay of 3 ns and 30 ns in DCM and 27 ns and 54 ns in the PMMA-doped film (Table **S3**). Therefore, **4PyCzBP-Pd** does not emit *via* a TADF mechanism but only from singlet excited states. DFT calculations reveal that the HOMO of **4PyCzBP-Pd** is mainly distributed over the twelve dipyridylcarbazolyl groups, as in the isolated dye (Figure **4c**). However, the LUMO of **4PyCzBP-Pd** is not localized on the benzophenone moiety as observed for the **4PyCzBP**, but it is primarily distributed on the six palladium atoms and their vicinal pyridyl units (Figure **4d**). As a result, the palladium ions act as electron acceptor units and quench the TADF nature of the **4PyCzBP** chromophores assembled within the structure of **4PyCzBP-Pd**.

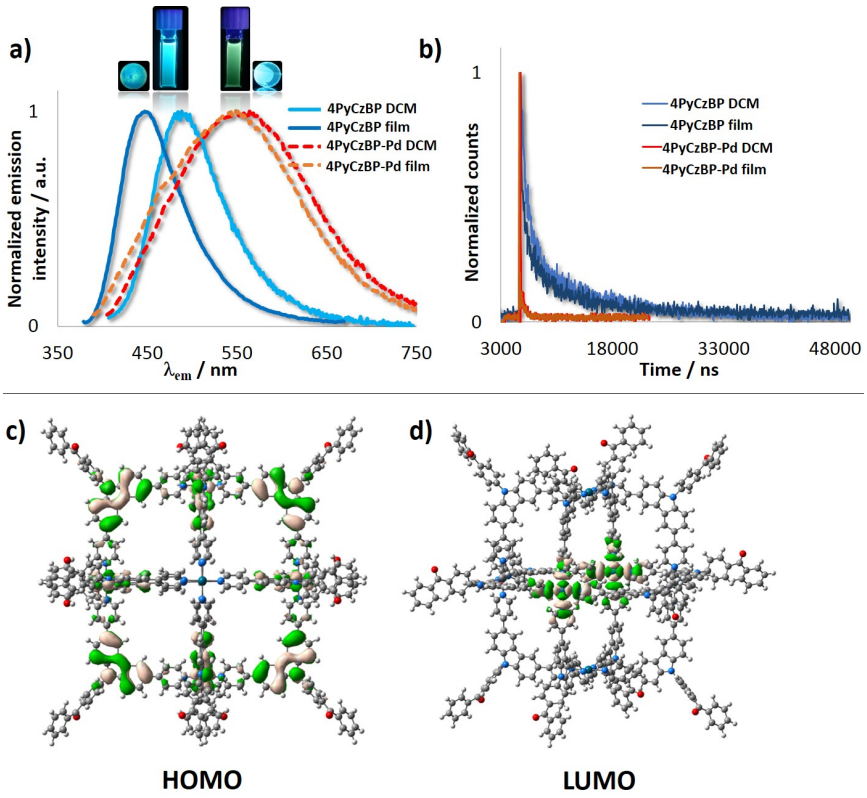

Figure **4**. **a)** Normalized emission spectra of **4PyCzBP** collected in deaerated DCM (solid light-blue line) and as a 10 wt% PMMA-film (solid blue-line) and of **4PyCzBP-Pd** collected in deaerated DCM (dotted red line) and as a 10 wt% PMMA-film (dotted orange line at 298 K. **b)** Emission decays of **4PyCzBP** in deaerated DCM (light-blue line) and in 10 wt% PMMA-film (blue-line) and of **4PyCzBP-Pd** collected in deaerated DCM (red line) and as a 10 wt% PMMA-film (orange line) at 298 K. DFT (CAM-B3LYP) calculated electron density distribution of **c)** HOMO level and **d)** LUMO level of **4PyCzBP-Pd**. Note that the HOMO and LUMO are each degenerated due to the high symmetry of the cage, and that only one representative MO is shown.

Xanthene dyes are widely used as pH sensor as they exist as colored quinone dianions (open form) at high pH (typically pH = 8 – 12) and as colorless lactones (closed form) at pH lower than 7.[50-51] Fujita *et al*. have recently demonstrated that the structural conversion of phthalein dyes can also be promoted through their encapsulation into the restricted cavity of cages, with

the spatial constraints pushing the equilibrium toward the formation of either the quinone dianions open form or the lactone closed form.[52]

In order to better understand the interplay between photoactive hosts and guests, two common xanthene dyes, fluorescein (F) and rose bengal (RB), were employed as guests. Notably, Ward *et al*. have recently demonstrated the encapsulation of F, Rhodamine and two other coumarin-based dyes into supramolecular polyhedral compartments of a crystalline zeolite framework, and have observed that the polyhedral cage prevented the dye monomers from aggregating.[53] Therefore, even at very high concentration, the emission of the encapsulated dyes is consistent with the presence of isolated monomeric species without any evidence of self-quenching.

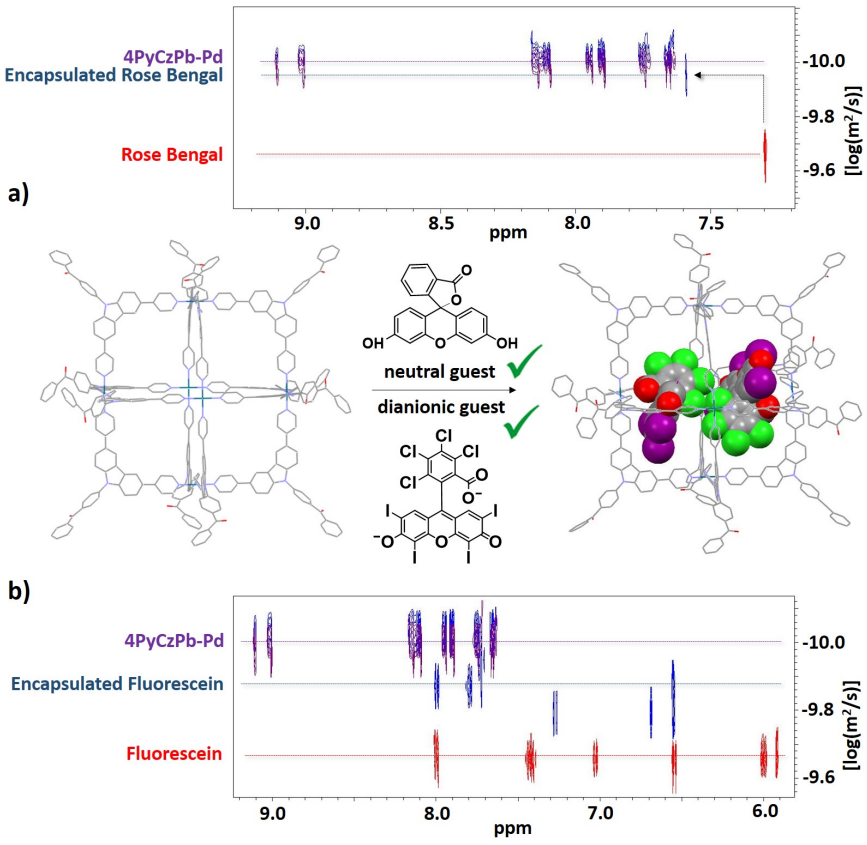

Figure **5**. **a)** Representation of encapsulation in DMSO-d_6 at room temperature of two molecules of RB within the cavity of **4PyCzBP-Pd**; including (top) the ^{1}H DOSY NMR spectra of RB (in red), **4PyCzBP-Pd** (in purple) and a 2:1 solution of RB and **4PyCzBP-Pd** (**4PyCzBP-Pd⊃(RB)**$_x$, (in blue). **b)** ^{1}H DOSY NMR spectra of F (in red), **4PyCzBP-Pd** (in purple) and a 2:1 solution of F and **4PyCzBP-Pd** (**4PyCzBP-Pd⊃(F)**$_x$, (in blue). The B3LYP-D3^{BJ}/6-31G(d)/LANL2DZ optimized host-guest structure **4PyCzBP-Pd⊃(RB)$_2$** is shown.

The calculated internal volume of **4PyCzBP-Pd** is suited to accommodate two guest RB molecules (Figure **5**). The binding of F and RB into the cavity of **4PyCzBP-Pd** was first examined. ^{1}H DOSY NMR analysis of a room temperature DMSO-d_6 solution containing one equivalent of the cage and two equivalents of either F and RB revealed a significant reduction of the diffusion coefficients of the guest molecules [$D_{(F)} = 1.9 \times 10^{-10}$ m^2/s, $D_{(RB)} = 1.8 \times 10^{-10}$ m^2/s] after mixing with **4PyCzBP-Pd** to form the host-guest assembly **4PyCzBP-Pd⊃(F)**$_x$ and **4PyCzBP-Pd⊃(RB)**$_x$ [$D_{(4PyCzBP-Pd⊃(F)x)} = 9.7 \times 10^{-11}$ m^2/s, $D_{(4PyCzBP-Pd⊃(RB)x)} = 9.4 \times 10^{-11}$ m^2/s, Figure **5**], with diffusion coefficients similar to that of **4PyCzBP-Pd** [$D_{(4PyCzBP-Pd)} = 9.1 \times 10^{-11}$ m^2/s]. The ^{1}H NMR spectra of **4PyCzBP-Pd⊃(F)**$_x$ and **4PyCzBP-Pd⊃(RB)**$_x$ showed that the resonances associated with the encapsulated dyes were significantly broadened and shifted downfield (Figures **S29**-**S30**). Electrospray ionization mass spectrometry (ESI-HRMS) experiments showed the presence of **4PyCzBP-Pd⊃(F)**$_{1-3}$ where one, two and three molecules of the neutral dye were encapsulated within the cavity of the cage (Figure **S13**-**S21**). The encapsulation of one and two molecules of RB into **4PyCzBP-Pd** (**4PyCzBP-Pd⊃(RB)**$_{1,2}$) was also detected by ESI-MS. However, RB is encapsulated as its quinoid dianionic form (Figure **S22**-**S26**) and, as it is larger than F, the encapsulation of a third molecule of RB within the cavity of **4PyCzBP-Pd** is sterically unfeasible. In order to ascertain whether **4PyCzBP-Pd** demonstrated selectivity for the encapsulation of F or RB, we collected the ESI-MS spectra of

a DMSO-d_6 mixture containing one equivalent of **4PyCzBP-Pd** and two equivalents of both guests. The ESI-MS spectra revealed a complicated mixture of host-guest systems of composition **4PyCzBP-Pd⊃(F)$_{1,2}$**, **4PyCzBP-Pd⊃(RB)$_{1,2}$**, **4PyCzBP-Pd⊃(F)$_1$(RB)$_1$** and **4PyCzBP-Pd⊃(F)$_2$(RB)$_1$** (Figure **S27**-**S28**).

Having confirmed that the cavity of **4PyCzBP-Pd** can accommodate F and RB, we turned our attention to the impact of encapsulation on the photophysical properties of the cage. UV-Visible spectra of F and RB in DMSO show, respectively, the yellow-green and pink colors characteristic of their dianion quinoid species.[54-56] A solution of **4PyCzBP-Pd** was added dropwise into the solutions of F and RB. Upon addition of **4PyCzBP-Pd** (from 0.1 to 3.0 equiv.) to the solution of F, the absorption band of F with a maximum at 522 nm, characteristic of its open quinoid form, significantly decreased. When three equivalents of **4PyCzBP-Pd** were added, the yellow-green solution became colorless (Figure **6a**). Therefore, the restricted cavity of **4PyCzBP-Pd** promotes the lactonization of F, which corroborates the presence of neutral fluorescein guest molecules by ESI-MS. Such behavior is analogous to that observed by Fujita *et al*.[52] who investigated the encapsulation of phthalein dyes within a tetrahedral cage. By contrast, when **4PyCzBP-Pd** (from 0.1 to 3.0 equiv.) was gradually added into a solution of RB, no change in intensity of the characteristic absorption band of this dye at 567 nm was observed (Figure **6b**), implying that this dye remains in its open dianion quinoid form upon encapsulation.

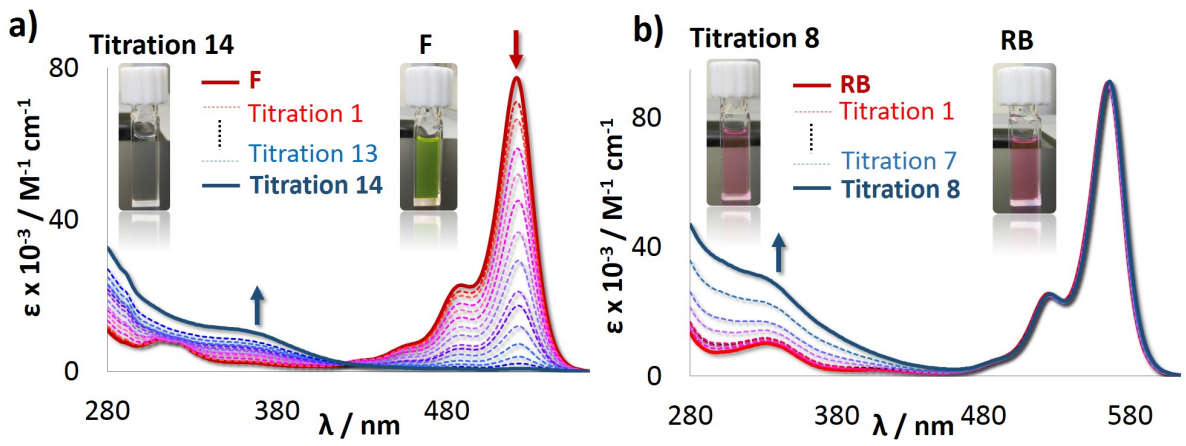

Figure **6**. **a)** UV-Vis titration of **F** (50 μM) after gradual addition of **4PyCzBP-Pd** (from 0 to 150 μM) in DMSO. **b)** UV-Vis titration of RB (50 μM) after gradual addition of **4PyCzBP-Pd** (from 0 to 150 μM) in DMSO. Photographs of solutions after addition of **4PyCzBP-Pd** (left) and initial solutions of dyes (right) are shown in the insets of each figure.

Emission titration experiments of **4PyCzBP-Pd** (from 0 to 150 μM) into a 50 μM degassed DMSO solution of either F or RB at 298 K were also carried out. When **4PyCzBP-Pd** was gradually added into the solution of F, a gradual quenching of the dye emission at 545 nm was observed, regardless of whether photoexcitation occurred at 360 nm (Figure **S37**), where both F and **4PyCzBP-Pd** both absorb, or at 480 nm (Figure **S38**), where only F absorbs. In both cases the emission of **4PyCzBP-Pd** was completely quenched. The quenching of the emission of F is attributed to its structural conversion toward the closed lactone form upon encapsulation.[52,55] However, the efficient quenching of the emission of **4PyCzBP-Pd** is ascribed to the formation of a non-emissive charge-separated state following PeT in **4PyCzBP-Pd**⊃(**F**)$_{1\text{-}3}$. The emission titration data was fitted to a 1:2 sequential binding model (Figure **S39**) with binding constant of K_b' of 7.8 × 10^3 ± 0.1 M^{-1} for the encapsulation of the first molecule of F, and K_b'' of 9.1 × 10^6 ± 0.5 M^{-1} for the encapsulation of the second and third guest molecule within the cavity of **4PyCzBP-Pd**. Fujita *et al*.[52] obtained a similar binding constant, K_b, of

approximately 10^7 M^{-1} for the encapsulation of one molecule of F into the cavity of their tetrahedral cage.

The redox properties of **4PyCzBP-Pd** and F were investigated by Cyclic Voltammetry (CV) and Differential Pulse Voltammetry (DPV) analyses (Figures **S33** and **S34**), and combined with optical data were used to estimate the energetics of the PeT processes in **4PyCzBP-Pd⊃F** (Figure **S35** and Table **S4**). The oxidation and reduction potentials of **4PyCzBP-Pd** are, respectively, at 1.76 and -1.63 V, whereas for F the oxidation potential is less positive at 0.67 V and the reduction potential is less negative at -1.08 V (Table **S4**). Therefore, the ground state electrochemical data suggests that for **4PyCzBP-Pd⊃F**, **F** is a better electron donor than **4PyCzBP-Pd** due to its higher ionization potential while **4PyCzBP-Pd** acts as the electron acceptor moiety.[57] The free energy (ΔG_{CS}) associated with the formation of the charge-separated state $[\mathbf{F}]^{\cdot+}[\mathbf{4PyCzBP\text{-}Pd}]^{\cdot-}$ was estimated from the Rehm-Weller equation[57] (see the SI for details) and was found to be exergonic at -0.39 eV and accounts for the quenching of the emission of **4PyCzBP-Pd**. Upon encapsulation of F into the cavity of a redox-active cobalt cage, Duan and *et al*. observed PeT from the excited state of F, there acting as the electron donor, to the redox-active cage.[58] By contrast, no optoelectronic communication was observed by Ward *et al*. between a F guest and a crystalline zeolite host.[53]

Emission titration of RB (from 0 to 150 μM) into a 50 μM degassed DMSO solution of **4PyCzBP-Pd** at 298 K resulted in a gradual quenching of the green emission of the donor **4PyCzBP-Pd** together with a gradual enhancement of the orange RB emission at 582 nm, with an isosbestic point observed at 561 nm (Figure **7a**). As a result, upon photoexcitation of **4PyCzBP-Pd⊃RB** at 360 nm, PET from **4PyCzBP-Pd** to RB is promoted. The binding constants determined from the emission titration study are K_b' of $9.2 \times 10^3 \pm 0.06$ M^{-1} for the encapsulation of the first molecule of RB and K_b'' of $1.8 \times 10^7 \pm 0.4$ M^{-1} for the encapsulation

of the second molecule of guest dye within the cavity of the cage (Figure **S40**). As electrostatic as well as non-covalent forces govern the binding of RB within **4PyCzBP-Pd**, the binding constants for the assembly **4PyCzBP-Pd⊃RB** are greater than those obtained for **4PyCzBP-Pd⊃F**. Our titration data also suggest that the encapsulation of two molecules of F is thermodynamically more favorable than the encapsulation of only one molecule of guest, which is consistent with the DFT computations (see the SI).

Stern-Volmer quenching analysis of **4PyCzBP-Pd⊃RB** demonstrated that the energy transfer/quenching process is very efficient,[59] with a calculated quenching rate constant (k_q) of 4.07 x 10^{11} $M^{-1}s^{-1}$ and a Stern-Volmer constant (K_{SV}) of 1.22 x 10^4 M^{-1} (Table **S5**). Due to the large spectral overlap (J = 1.41 x 10^{12} $nm^4\,M^{-1}\,cm^{-1}$) between the absorption of RB and the emission of **4PyCzBP-Pd** (Figure **S41**), Förster energy transfer is the likely mechanism for the energy transfer in system. The *Commission Internationale de l'Éclairage*, CIE, diagram shown in Figure **7b** illustrates the change in the emission colors observed during the emission titration. Importantly, by manipulating the concentration of the host **4PyCzBP-Pd** and guest RB, we developed a white-light emitting assembly with CIE coordinates of (0.32, 0.34), which are close to coordinates of the pure white light (x: 0.31, y: 0.33).

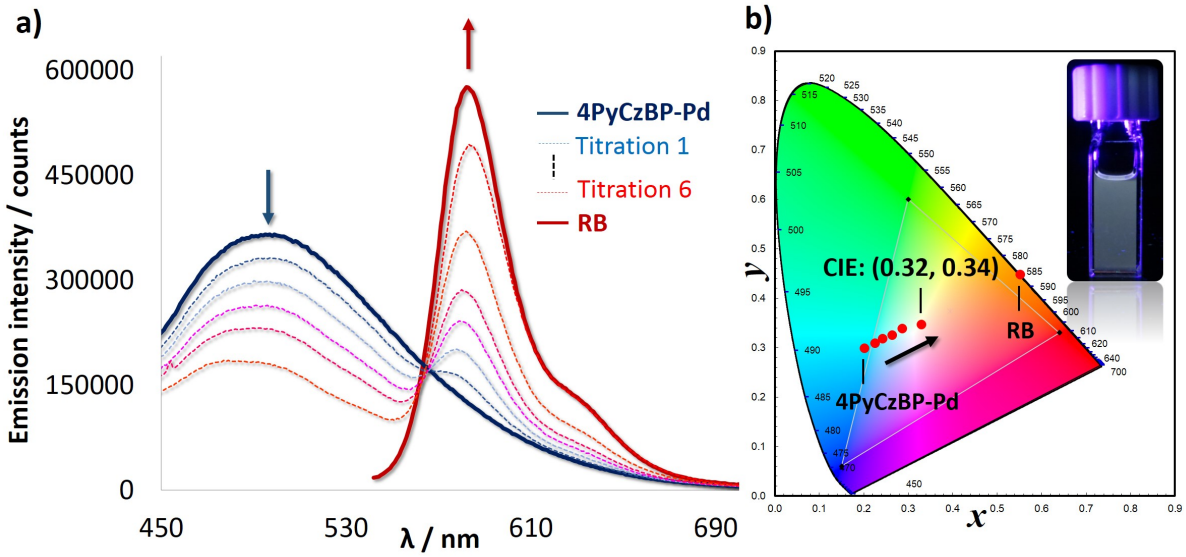

Figure **7**. **a)** Emission titrations of **RB** (from 0 μM to 150 μM) into a 50 μM solution of **4PyCzBP-Pd** at 298 K in degassed DMSO. **b)** CIE diagram indicating the change of emission colors during the emission titration. Photograph of the white-emitting solution with CIE coordinates (x: 0.32, y: 0.34) is shown in the inset of the spectrum.

Conclusions.

In summary, a luminescent supramolecular $[Pd_6L_{12}](BF_4)_{12}$ cage has been prepared by self-assembly of Pd^{2+} ions with a TADF ligand **4PyCzBP**. **4PyCzBP-Pd** is able to encapsulate up to up to three molecules of Fluorescein, in its closed lactone form, and up to two molecules of Rose Bengal, in its open quinoid form. Examples of efficient energy or electron transfer between luminescent guests and photoactive cages are rare. In the present study we showed that PeT between the encapsulated fluorescein and the cage **4PyCzBP-Pd** and PET from **4PyCzBP-Pd** to encapsulated Rose Bengal occur. These assemblies open up the possibility of exploiting these interactions in photocatalysis, examples of which are exceedingly rare.

Acknowledgements. We thank the Leverhulme Trust (RPG-2016-047) and EPSRC (EP/P010482/1) for financial support. DE thanks funding from the European Union's Horizon 2020 research and innovation programme under the Marie Sklodowska-Curie grant agreement No. 700961.We thank Umicore Ag for the gift of the Pd(II) salts. We thank the EPSRC UK National Mass Spectrometry Facility at Swansea University for analytical services. This work uses computational resources of the CCIPL installed in Nantes.

Supporting information. Experimental section, characterization of ligands and cages, supplementary optoelectronic data and supplementary computational details.

References.

(1) Chakrabarty, R.; Mukherjee, P. S.; Stang, P. J., Supramolecular Coordination: Self-Assembly of Finite Two- and Three-Dimensional Ensembles. *Chem. Rev.* **2011**, *111*, 6810.
(2) Smulders, M. M. J.; Riddell, I. A.; Browne, C.; Nitschke, J. R., Building on Architectural Principles for Three-dimensional Metallosupramolecular Construction. *Chem. Soc. Rev.* **2013**, *42*, 1728.
(3) Fujita, D.; Ueda, Y.; Sato, S.; Mizuno, N.; Kumasaka, T.; Fujita, M., Self-assembly of Tetravalent Goldberg Polyhedra from 144 Small Components. *Nature* **2016**, *540*, 563.
(4) Fujita, D.; Ueda, Y.; Sato, S.; Yokoyama, H.; Mizuno, N.; Kumasaka, T.; Fujita, M., Self-Assembly of M30L60 Icosidodecahedron. *Chem* **2016**, *1*, 91.
(5) Han, M.; Engelhard, D. M.; Clever, G. H., Self-assembled Coordination Cages Based on Banana-shaped Ligands. *Chem Soc Rev* **2014**, *43*, 1848.
(6) Zhang, Y.-Y.; Gao, W.-X.; Lin, L.; Jin, G.-X., Recent Advances in the Construction and Applications of Heterometallic Macrocycles and Cages. *Coord. Chem. Rev.* **2017**, *344*, 323.
(7) Wang, W.; Wang, Y. X.; Yang, H. B., Supramolecular Transformations Within Discrete Coordination-driven Supramolecular Architectures. *Chem Soc Rev* **2016**, *45*, 2656.
(8) Zarra, S.; Wood, D. M.; Roberts, D. A.; Nitschke, J. R., Molecular Containers in Complex Chemical Systems. *Chem Soc Rev* **2015**, *44*, 419.
(9) August, D. P.; Nichol, G. S.; Lusby, P. J., Maximizing Coordination Capsule-Guest Polar Interactions in Apolar Solvents Reveals Significant Binding. *Angew Chem Int Ed Engl* **2016**, *55*, 15022.
(10) Ronson, T. K.; Zarra, S.; Black, S. P.; Nitschke, J. R., Metal-organic Container Molecules Through Subcomponent Self-assembly. *Chem. Commun.* **2013**, *49*, 2476.
(11) Yoshizawa, M.; Miyagi, S.; Kawano, M.; Ishiguro, K.; Fujita, M., Alkane Oxidation via Photochemical Excitation of a Self-Assembled Molecular Cage. *J. Am. Chem. Soc.* **2004**, *126*, 9172.
(12) Li, X.; Wu, J.; Chen, L.; Zhong, X.; He, C.; Zhang, R.; Duan, C., Engineering an Iridium-Containing Metal-organic Molecular Capsule for Induced-fit Geometrical Conversion and Dual Catalysis. *Chem. Commun.* **2016**, *52*, 9628.
(13) Yan, L. L.; Tan, C. H.; Zhang, G. L.; Zhou, L. P.; Bunzli, J. C.; Sun, Q. F., Stereocontrolled Self-Assembly and Self-Sorting of Luminescent Europium Tetrahedral Cages. *J Am Chem Soc* **2015**, *137*, 8550.
(14) Li, X. Z.; Zhou, L. P.; Yan, L. L.; Yuan, D. Q.; Lin, C. S.; Sun, Q. F., Evolution of Luminescent Supramolecular Lanthanide M2nL3n Complexes from Helicates and Tetrahedra to Cubes. *J Am Chem Soc* **2017**, *139*, 8237.
(15) Dong, Y.-B.; Wang, P.; Ma, J.-P.; Zhao, X.-X.; Wang, H.-Y.; Tang, B.; Huang, R.-Q., Coordination-Driven Nanosized Lanthanide "Molecular Lantern" with Tunable Luminescent Properties. *J. Am. Chem. Soc.* **2007**, *129*, 4872.
(16) Frischmann, P. D.; Kunz, V.; Wurthner, F., Bright Fluorescence and Host-Guest Sensing with a Nanoscale M(4)L(6) Tetrahedron Accessed by Self-Assembly of Zinc-Imine Chelate Vertices and Perylene Bisimide Edges. *Angew Chem Int Ed Engl* **2015**, *54*, 7285.
(17) Kishi, N.; Akita, M.; Yoshizawa, M., Selective Host-guest Interactions of a Transformable Coordination Capsule/tube with Fullerenes. *Angew Chem Int Ed Engl* **2014**, *53*, 3604.
(18) Fan, W.-J.; Sun, B.; Ma, J.; Li, X.; Tan, H.; Xu, L., Coordination-Driven Self-Assembly of Carbazole-Based Metallodendrimers with Generation-Dependent Aggregation-Induced Emission Behavior. *Chem. Eur. J.* **2015**, *21*, 12947.
(19) Kishi, N.; Li, Z.; Sei, Y.; Akita, M.; Yoza, K.; Siegel, J. S.; Yoshizawa, M., Wide-ranging Host Capability of a Pd(II)-linked M2L4 Molecular Capsule with an Anthracene Shell. *Chem. Eur. J.* **2013**, *19*, 6313.

(20) Xu, L.; Wang, Y. X.; Yang, H. B., Recent Advances in the Construction of Fluorescent Metallocycles and Metallocages via Coordination-driven Self-assembly. *Dalton Trans* **2015**, *44*, 867.
(21) Frank, M.; Ahrens, J.; Bejenke, I.; Krick, M.; Schwarzer, D.; Clever, G. H., Light-Induced Charge Separation in Densely Packed Donor-Acceptor Coordination Cages. *J Am Chem Soc* **2016**, *138*, 8279.
(22) Durot, S.; Taesch, J.; Heitz, V., Multiporphyrinic cages: Architectures and Functions. *Chem Rev* **2014**, *114*, 8542.
(23) Neelakandan, P. P.; Jimenez, A.; Nitschke, J. R., Fluorophore Incorporation Allows Nanomolar Guest Sensing and White-light Emission in M4L6 Cage Complexes. *Chem. Sci.* **2014**, *5*, 908.
(24) Rota Martir, D.; Escudero, D.; Jacquemin, D.; Cordes, D. B.; Slawin, A. M. Z.; Fruchtl, H. A.; Warriner, S. L.; Zysman-Colman, E., Homochiral Emissive Λ8- and Δ8-[Ir8Pd4]16+ Supramolecular Cages. *Chem. Eur. J.*, *23,* 14358.

(25) Chepelin, O.; Ujma, J.; Wu, X.; Slawin, A. M. Z.; Pitak, M. B.; Coles, S. J.; Michel, J.; Jones, A. C.; Barran, P. E.; Lusby, P. J., Luminescent, Enantiopure, Phenylatopyridine Iridium-Based Coordination Capsules. *J. Am. Chem. Soc.* **2012**, *134*, 19334.
(26) Pritchard, V. E.; Rota Martir, D.; Oldknow, S.; Kai, S.; Hiraoka, S.; Cookson, N. J.; Zysman-Colman, E.; Hardie, M. J., Homochiral Self-Sorted and Emissive IrIII Metallo-Cryptophanes. *Chem. Eur. J.* **2017**, *23*, 6290.
(27) Yang, J.; Bhadbhade, M.; Donald, W. A.; Iranmanesh, H.; Moore, E. G.; Yan, H.; Beves, J. E., Self-assembled Supramolecular Cages Containing Ruthenium(II) Polypyridyl Complexes. *Chem. Commun.* **2015**, *51*, 4465.
(28) Chen, S.; Li, K.; Zhao, F.; Zhang, L.; Pan, M.; Fan, Y. Z.; Guo, J.; Shi, J.; Su, C. Y., A Metal-organic Cage Incorporating Multiple Light Harvesting and Catalytic Centres for Photochemical Hydrogen Production. *Nat Commun* **2016**, *7*, 13169.
(29) Li, K.; Zhang, L. Y.; Yan, C.; Wei, S. C.; Pan, M.; Zhang, L.; Su, C. Y., Stepwise Assembly of Pd(6)(RuL(3))(8) Nanoscale Rhombododecahedral Metal-organic Cages via Metalloligand Strategy for guest trapping and Protection. *J Am Chem Soc* **2014**, *136*, 4456.
(30) Yan, X.; Wang, M.; Cook, T. R.; Zhang, M.; Saha, M. L.; Zhou, Z.; Li, X.; Huang, F.; Stang, P. J., Light-Emitting Superstructures with Anion Effect: Coordination-Driven Self-Assembly of Pure Tetraphenylethylene Metallacycles and Metallacages. *J Am Chem Soc* **2016**, *138*, 4580.
(31) Yan, X.; Cook, T. R.; Wang, P.; Huang, F.; Stang, P. J., Highly Emissive Platinum(II) Metallacages. *Nat Chem* **2015**, *7*, 342.
(32) Nakamura, T.; Ube, H.; Shionoya, M., Silver-mediated Formation of a Cofacial Porphyrin Dimer with the Ability to Intercalate Aromatic Molecules. *Angew Chem Int Ed Engl* **2013**, *52*, 12096.
(33) Shanmugaraju, S.; Jadhav, H.; Patil, Y. P.; Mukherjee, P. S., Self-assembly of an Octanuclear Platinum(II) Tetragonal Prism from a New Pt(II)4 Organometallic Star-shaped Acceptor and its Nitroaromatic Sensing Study. *Inorg Chem* **2012**, *51*, 13072.
(34) Wang, J.; He, C.; Wu, P.; Wang, J.; Duan, C., An Amide-containing Metal-organic Tetrahedron Responding to a Spin-trapping Reaction in a Fluorescent Enhancement Manner for Biological Imaging of NO in Iiving Cells. *J Am Chem Soc* **2011**, *133*, 12402.
(35) Kishi, N.; Akita, M.; Kamiya, M.; Hayashi, S.; Hsu, H. F.; Yoshizawa, M., Facile Catch and Release of Fullerenes Using a Photoresponsive Molecular Tube. *J Am Chem Soc* **2013**, *135*, 12976.

(36) Han, M.; Michel, R.; He, B.; Chen, Y. S.; Stalke, D.; John, M.; Clever, G. H., Light-triggered Guest Uptake and Release by a Photochromic Coordination Cage. *Angew Chem Int Ed Engl* **2013**, *52*, 1319.
(37) Zhu, R.; Lubben, J.; Dittrich, B.; Clever, G. H., Stepwise Halide-triggered Double and Triple Catenation of Self-assembled Coordination Cages. *Angew Chem Int Ed Engl* **2015**, *54*, 2796.
(38) Wong, M. Y.; Zysman-Colman, E., Purely Organic Thermally Activated Delayed Fluorescence Materials for Organic Light-Emitting Diodes. *Adv Mater* **2017**, *29*, 1605444.
(39) Yang, Z.; Mao, Z.; Xie, Z.; Zhang, Y.; Liu, S.; Zhao, J.; Xu, J.; Chi, Z.; Aldred, M. P., Recent Advances in Organic Thermally Activated Delayed Fluorescence Materials. *Chem. Soc. Rev.* **2017**, *46*, 915.
(40) Im, Y.; Kim, M.; Cho, Y. J.; Seo, J.-A.; Yook, K. S.; Lee, J. Y., Molecular Design Strategy of Organic Thermally Activated Delayed Fluorescence Emitters. *Chem. Mater.* **2017**, *29*, 1946.
(41) Wex, B.; Kaafarani, B. R., Perspective on Carbazole-based Organic Compounds as Emitters and Hosts in TADF Applications. *J. Mater. Chem. C* **2017**, *5*, 8622.
(42) Uoyama, H.; Goushi, K.; Shizu, K.; Nomura, H.; Adachi, C., Highly Efficient Organic Light-emitting Diodes from Delayed Fluorescence. *Nature* **2012**, *492*, 234.
(43) Rajamalli, P.; Martir, D. R.; Zysman-Colman, E., Molecular Design Strategy for a Two-Component Gel Based on a Thermally Activated Delayed Fluorescence Emitter. *ACS Applied Energy Materials* **2018**, *1*, 649.
(44) Rajamalli, P.; Martir, D. R.; Zysman-Colman, E., Pyridine-functionalized Carbazole Donor and Benzophenone Acceptor Design for Thermally Activated Delayed Fluorescence Emitters in Blue Organic Light-emitting Diodes. *J. Photon Energy* **2018**, *8*, 26.
(45) Suzuki, K.; Tominaga, M.; Kawano, M.; Fujita, M., Self-assembly of an M6L12 Coordination Cube. *Chem. Commun.* **2009**, 1638.
(46) Sun, Q.-F.; Iwasa, J.; Ogawa, D.; Ishido, Y.; Sato, S.; Ozeki, T.; Sei, Y.; Yamaguchi, K.; Fujita, M., Self-Assembled M24L48 Polyhedra and Their Sharp Structural Switch upon Subtle Ligand Variation. *Science* **2010**, *328*, 1144.
(47) Ni, Z.; Yassar, A.; Antoun, T.; Yaghi, O. M., Porous Metal–Organic Truncated Octahedron Constructed from Paddle-Wheel Squares and Terthiophene Links. *J. Am. Chem. Soc.* **2005**, *127*, 12752.
(48) Perry; Kravtsov, V. C.; McManus, G. J.; Zaworotko, M. J., Bottom up Synthesis That Does Not Start at the Bottom: Quadruple Covalent Cross-Linking of Nanoscale Faceted Polyhedra. *J. Am. Chem. Soc.* **2007**, *129*, 10076.
(49) Liu, Y.; Kravtsov, V. C.; Beauchamp, D. A.; Eubank, J. F.; Eddaoudi, M., 4-Connected Metal–Organic Assemblies Mediated via Heterochelation and Bridging of Single Metal Ions: Kagomé Lattice and the M6L12 Octahedron. *J. Am. Chem. Soc.* **2005**, *127*, 7266.
(50) Berger, S., The pH Dependence of Phenolphthalein: A 13C NMR Study. *Tetrahedron* **1981**, *37*, 1607.
(51) Kunimoto, K.-K.; Sugiura, H.; Kato, T.; Senda, H.; Kuwae, A.; Hanai, K., Molecular Structure and Vibrational Spectra of Phenolphthalein and its Dianion. *Spectrochimica Acta Part A: Molecular and Biomolecular Spectroscopy* **2001**, *57*, 265.
(52) Takezawa, H.; Akiba, S.; Murase, T.; Fujita, M., Cavity-Directed Chromism of Phthalein Dyes. *J Am Chem Soc* **2015**, *137*, 7043.
(53) Handke, M.; Adachi, T.; Hu, C.; Ward, M. D., Encapsulation of Isolated Luminophores within Supramolecular Cages. *Angew. Chem. Int. Ed., ASAP*, DOI: 10.1002/anie.201707097.
(54) Slyusareva, E. A.; Gerasimova, M. A., pH-Dependence of the Absorption and Fluorescent Properties of Fluorone Dyes in Aqueous Solutions. *Russian Physics Journal* **2014**, *56*, 1370.

(55) Sjöback, R.; Nygren, J.; Kubista, M., Absorption and Fluorescence Properties of Fluorescein. *Spectrochimica Acta Part A: Molecular and Biomolecular Spectroscopy* **1995**, *51*, L7.
(56) Chang, C.-C.; Yang, Y.-T.; Yang, J.-C.; Wu, H.-D.; Tsai, T., Absorption and Emission Spectral Shifts of Rose Bengal Associated with DMPC Liposomes. *Dyes and Pigments* **2008**, *79*, 170.
(57) Kavarnos, G. J.; Turro, N. J., Photosensitization by Reversible Electron Transfer: Theories, Experimental Evidence, and Examples. *Chem. Rev.* **1986**, *86*, 401.
(58) Jing, X.; He, C.; Yang, Y.; Duan, C., A Metal-organic Tetrahedron as a Redox Vehicle to Encapsulate Organic Dyes for Photocatalytic Proton Reduction. *J Am Chem Soc* **2015**, *137*, 3967.
(59) Kirk, A. D.; Namasivayam, C., Reversible Energy Transfer Between Chromium(III) Complexes. *J. Phys. Chem.* **1989**, *93*, 5488.

TOC Graphic.